Simulation of the Propagation of Surface Gravity Waves Using Local Polynomial Approximation

Andrew B. Kennedy and John D. Fenton
Department of Mechanical Engineering, Monash University
Clayton, Victoria, Australia 3168

Summary A numerical method is developed to model the propagation of gravity waves over varying topography. The representation of the velocity potential by a local polynomial approximation of arbitrary order provides an accurate and efficient solution to Laplace's equation for one dimension in plan. The full nonlinear free surface evolution equations are then directly applied to advance the solution in time. Energy is conserved to a high degree in the included examples of a propagating solitary wave, colliding solitary waves, and a shoaling solitary wave, giving an independent verification of accuracy.

Introduction

The propagation of surface gravity waves over varying topography has long been studied. Many approximate solutions to the equations of motion have been developed, but all suffer from limitations. The shallow water equations are well known but cannot describe steady, progressive waves, and are unsuitable for many problems of engineering interest. Boussinesq equations (Peregrine, 1967, Nwogu, 1993, others) can model waves which are both steady and progressive, and extend the practical computational range, but are only mildly nonlinear and lose accuracy as both wave height and water depth increase. The KdV equation (Korteweg and de Vries, 1895, Johnson, 1973) suffers from similar problems. Boundary integral methods (Longuet-Higgins and Cokelet, 1976, Grilli et al, 1994, others) can provide excellent accuracy for any wave height in any water depth and may even be used to describe overturning waves, but are extremely expensive computationally. Fourier solutions of the full equations of motion can offer good accuracy, but assume a periodic domain, and most are computationally expensive (Multer, 1973, Fenton and Rienecker, 1982). The Fourier method of Dommermuth and Yue (1987) is highly efficient, but is somewhat difficult to implement for anything other than a level topography.

In this paper, a method is developed in the time domain for nonbreaking wave propagation in finite depths for one dimension in plan. Potential flow is assumed. The centrepiece of this method is a solution of Laplace's equation using local polynomial approximation (LPA, see Fenton, 1986) of arbitrary order. Due to the use of a local instead of global representation of the velocity potential, the time of solution is directly proportional to the number of computational subdomains. This can provide an excellent combination of accuracy and efficiency, as will be shown.

Governing Equations

Irrotational flow in an inviscid, incompressible fluid may be described by a velocity potential $\phi(x,y,t)$, such that, for one dimension in plan, the fluid velocity vector $(u,v) = (\partial\phi/\partial x, \partial\phi/\partial y)$, where x and y are, respectively, the horizontal and vertical coordinates, and t is time. Throughout the fluid domain, the velocity potential must satisfy Laplace's equation:

$$\nabla^2\phi = 0, \tag{1}$$

while, on the solid, motionless, bed, the bottom boundary condition must be satisfied. This may be written as

$$\frac{\partial\phi}{\partial y} - \frac{\partial h}{\partial x}\frac{\partial\phi}{\partial x} = 0 \quad \text{on } y = h, \tag{2}$$

where $h(x)$ is the vertical bed coordinate. The dynamic free surface boundary condition is the unsteady form of Bernoulli's equation:

$$\frac{\partial\phi}{\partial t} + \frac{1}{2}(u^2 + v^2) + g\eta + \frac{p}{\rho} = C \quad \text{on } y = \eta, \tag{3}$$

where $\eta(x,t)$ is the location of the free surface, g is gravitational acceleration, p is the pressure, which will be taken to be zero at the free surface, and ρ is the fluid density. $C(t)$ is a constant throughout space. The kinematic free surface boundary condition is

$$\frac{\partial\eta}{\partial t} - \frac{\partial\phi}{\partial y} + \frac{\partial\eta}{\partial x}\frac{\partial\phi}{\partial x} = 0 \quad \text{on } y = \eta, \tag{4}$$

and is the equivalent of the bottom boundary condition for a moving boundary.

Problem Definition

Consider the situation shown in Figure 1. Nonbreaking surface gravity waves propagate in one dimension in plan over varying topography with no discontinuities in bottom elevation. At time t=0, both the elevation and velocity potential are known at selected unevenly spaced points along the free surface, and global boundary conditions are known. Once the field equation (1) is solved, subject to boundary condition (2), equations (3) and (4) may be used to advance the free surface in time.

However, although the solution of Laplace's equation in two dimensions is a potentially arduous task, in finite water depths it is possible to make assumptions about the structure of the flow which allow for an accurate and highly efficient solution.

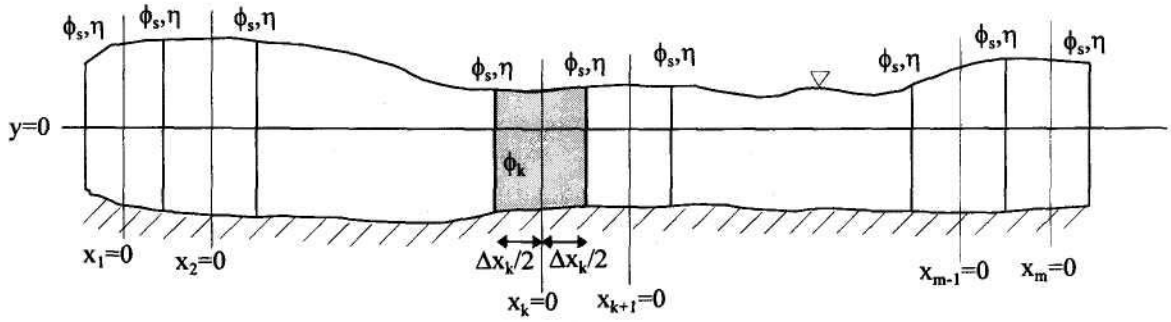

Figure 1. Definition sketch for wave motion

Solution of Laplace's Equation

Consider the velocity potential function satisfying (1)

$$\phi_k(x,y,t)=\left[A_{0R}+\mathrm{Re}\left(\begin{array}{l}\left(\sum_{j=1}^{n-1}(A_{jR}+iA_{jI})(x_k+iy)^j\right)\\ +(x_k+iy)^n\times\begin{cases}A_{nR}, & n \text{ odd}\\ iA_{nI}, & n \text{ even}\end{cases}\end{array}\right)\right]_k, \quad (5)$$

where Re indicates the real part of a complex expression, $i=\sqrt{-1}$, n is an arbitrary integer greater than or equal to 2, and the A coefficients are independent and may vary in time. This function is defined only in region k, with local coordinates as shown in Figure 1. If $n=2$, the velocity potential will have the same vertical structure as the shallow water equations. For $n=3$, it will have the same vertical structure as the Boussinesq equations. It would seem reasonable that larger values of n could give a better approximation to the actual velocity potential function and enable the description of more complex flows.

Although (5) is the most straightforward representation of ϕ_k, another equivalent form is to be preferred, for reasons which will shortly become clear. The new form will be

$$\phi_k(x,y,t)=\left[\sum_{j=0}^{n-1}(B_{jL}\phi_{jL}(x_k,y)+B_{jR}\phi_{jR}(x_k,y))\right]_k, \quad (6)$$

where B_{jL} and B_{jR} are independent coefficients which may vary in time. ϕ_{jL} and ϕ_{jR} are independent subsets of ϕ_k defined such that

$$\phi_{jL}=\begin{cases}y^j, & x_k=-\Delta x_k/2\\ 0, & x_k=\Delta x_k/2\end{cases}$$
$$\phi_{jR}=\begin{cases}0, & x_k=-\Delta x_k/2\\ y^j, & x_k=\Delta x_k/2\end{cases}. \quad (7)$$

To find this form, expand (5) using the binomial theorem and collect like powers of y. For constant x_k, the velocity potential is now a simple polynomial in y of degree n-1, with the magnitude of each term dependent on the A coefficients. If ϕ_k is represented in this manner at $x_k=\pm\Delta x_k/2$, the form of (6) and (7) may be found in a straightforward manner by creating a matrix equation in A_{jR} and A_{jI} with a different right hand side for each ϕ_{jL} and ϕ_{jR}.

Finally, it should be noted that since ϕ_{jL}, ϕ_{jR} and their spatial derivatives are all, for constant x_k, simple polynomials in y, it is possible to create one dimensional representations of these functions which are simpler to calculate. If this is done at $x_k=\pm\Delta x_k/2$, much computational expense will be saved, as they will frequently be evaluated at these locations.

Now that the form of the velocity potential has been established, it is necessary to find $2n$ conditions to uniquely determine the function over area k or, in an equivalent sense over the whole domain, $2n$ conditions at each interior boundary, plus n conditions at each of the left and right global boundaries. Consider the interior boundary between areas k and k+1, as shown in Figure 1. If ϕ is to be continuous across the boundary

$$\left(\sum_{j=0}^{n-1}B_{jR}\phi_{jR}\right)_k=\left(\sum_{j=0}^{n-1}B_{jL}\phi_{jL}\right)_{k+1}. \quad (8)$$

It is obvious from (7) that $(B_{jR})_k=(B_{jL})_{k+1}$. These n continuity conditions may be implicitly implemented by using $B_{j,k}=(B_{jR})_k=(B_{jL})_{k+1}$ as a new coefficient. η will now be continuous across the boundary to the zeroth order without any explicit arguments.

Another condition may be filled by setting ϕ at the free surface to the known ϕ_s. The bottom boundary condition (2) must also be imposed, using the average value of $\partial\phi/\partial x$ across the boundary.

There are n-2 conditions which remain to be defined at each interior boundary. To fill these, the difference in $\partial\phi/\partial x$ across the boundary is set to zero at n-2 discrete points. A possible choice of location would be the Chebyshev points, but here, they are instead chosen to be the Gauss-Legendre quadrature points for N=n-2, with the upper and lower limits taken to be the free surface and the bed. For $n\geq 5$, this will ensure that $q_\pm=0$, where

$$q_\pm=\int_h^\eta(u_+-u_-)dy, \quad (9)$$

		Δu_{RMS}		
H/d	n	$m=15$	$m=30$	$m=60$
	3	4.4×10^{-3}	1.1×10^{-3}	1.4×10^{-3}
0.1	7	8.8×10^{-5}	1.9×10^{-6}	2.3×10^{-7}
	11	1.5×10^{-5}	6.4×10^{-9}	5.0×10^{-11}
	3	1.4×10^{-2}	4.8×10^{-3}	4.7×10^{-3}
0.3	7	1.1×10^{-3}	3.3×10^{-5}	3.9×10^{-6}
	11	1.0×10^{-4}	4.1×10^{-6}	5.0×10^{-9}
	3	2.3×10^{-2}	9.5×10^{-3}	8.5×10^{-3}
0.5	7	1.2×10^{-3}	1.3×10^{-4}	1.5×10^{-5}
	11	1.2×10^{-3}	1.1×10^{-5}	1.7×10^{-7}
	3	2.7×10^{-2}	2.0×10^{-2}	1.3×10^{-2}
0.7	7	7.9×10^{-3}	4.1×10^{-3}	4.2×10^{-4}
	11	1.1×10^{-2}	3.0×10^{-3}	7.6×10^{-5}
		(a) $L/d=20$		

		Δu_{RMS}		
H/d	n	$m=15$	$m=30$	$m=60$
	3	2.3×10^{-2}	2.4×10^{-2}	2.5×10^{-2}
0.1	7	2.0×10^{-5}	3.8×10^{-6}	9.1×10^{-7}
	11	2.8×10^{-8}	1.2×10^{-9}	1.9×10^{-10}
	3	2.6×10^{-2}	2.6×10^{-2}	2.6×10^{-2}
0.3	7	6.3×10^{-5}	1.2×10^{-5}	2.9×10^{-6}
	11	9.0×10^{-7}	1.1×10^{-8}	1.5×10^{-9}
	3	3.1×10^{-2}	2.9×10^{-2}	2.9×10^{-2}
0.45	7	2.9×10^{-4}	5.3×10^{-5}	1.2×10^{-5}
	11	1.7×10^{-5}	1.6×10^{-6}	1.9×10^{-7}
		(b) $L/d=5$		

		Δu_{RMS}		
H/d	n	$m=15$	$m=30$	$m=60$
	3	1.2×10^{-1}	1.2×10^{-1}	1.2×10^{-1}
0.1	7	1.7×10^{-4}	4.0×10^{-5}	9.9×10^{-6}
	11	3.3×10^{-7}	6.0×10^{-8}	1.4×10^{-8}
	3	1.0×10^{-1}	1.0×10^{-1}	1.0×10^{-1}
0.2	7	3.7×10^{-4}	8.5×10^{-5}	5.2×10^{-5}
	11	2.1×10^{-5}	2.7×10^{-6}	5.7×10^{-7}
		(c) $L/d=2$		

Table 1. LPA fit to a regular wave

and the subscripts indicate the right and left sides of the boundary, respectively.

If the domain is periodic, then global boundaries may simply be treated in the same manner as internal boundaries but, otherwise, a somewhat different approach is needed. At each boundary, n conditions must be given. Two of these will always be the specification of the free surface velocity potential, and the imposition of the bottom boundary condition (2). The remaining n-2 conditions may be filled through the specification of known velocity potentials and/or velocities at discrete points. For the case of a vertical wall, which will be used here for all computations of wave propagation, horizontal velocities are set to zero at the Gauss-Legendre points.

There are now as many equations as unknowns, and the resulting linear system of equations may be solved using a banded matrix solver. As previously stated, this provides the "order m" solution which is the major advantage of LPA.

Representation of the Free Surface and Bed

Bed and surface slopes are generally found using finite differences, but here, both were represented using simple one dimensional polynomial splines (normally of degree n) with break points coincident with the internal and external boundaries. Since the computational grid remained constant in time, a solution matrix was computed only once, with the consequent savings. For a global boundary condition of a vertical wall, odd spatial derivatives were set to zero.

Time Stepping Procedure

Once the velocity potential function has been determined, (3) and (4) may be used to advance the system in time. Equation (4) may be applied directly, while (3) changes somewhat to become

$$\frac{\partial \phi_s}{\partial t} = C - g\eta - \frac{1}{2}\left(\left(\frac{\partial \phi}{\partial x}\right)^2 + \left(\frac{\partial \phi}{\partial y}\right)^2\right) + \frac{\partial \phi}{\partial y}\frac{\partial \eta}{\partial t} \quad \text{on } y=\eta, \quad (10)$$

the rate of change of ϕ for a particle constrained in the x-direction but moving with the free surface. For all calculations presented here, a fourth order Adams-Bashforth time stepping technique (AB4) was used, since it provided reasonable accuracy while requiring no intermediate steps, which would have been extremely costly. As the AB4 method is not self starting, a fourth order Runge-Kutta technique was used for the first three time steps.

Approximation of Velocity Potential Function for a Regular Wave

To test the accuracy of LPA solutions of Laplace's Equation, discrete values of surface elevation and velocity potential were used to generate LPA velocity potential functions which were then compared with the exact solutions. Elevations and potentials used as input were taken from waves generated using numerical Fourier theory (Rienecker and Fenton (1981), Fenton (1988)), which gives an accurate waveform and, as importantly, provides an exact solution of Laplace's equation throughout the domain.

A "goodness of fit" parameter was generated for each wave tested. At each evenly spaced computational point, the difference in velocities between the exact solution and LPA was found for u_s, v_s, and u_b. The subscripts here represent, respectively, the free surface and the bed, and horizontal velocities were averaged across the boundary. The root mean square (RMS) value of all of these differences was then divided by the exact maximum u_s at any computational point to give Δu_{RMS}, the dimensionless RMS velocity difference. Table 1 gives Δu_{RMS} for various dimensionless wavelength to depth ratios L/d and heights H/d.

As expected, accuracy tends to increase with increasing degree of polynomial, n. Errors also tend to

decrease with increasing number of computational subdomains, m, but, as may be seen with the results for n=3, a limit is reached as n itself limits the complexity of flow. However, with the right combination of n and m, almost any desired level of accuracy may be achieved, even with the highest waves tested. Most impressively for what is essentially a shallow water expansion, this applies up to the deep water limit of $L/d = 2$.

The use of n values much greater than 11 may require special techniques, as the large exponents make the matrix equations somewhat ill-conditioned. Using n=11, the potential accuracy of LPA could, in some cases, exceed the accuracy of the matrix solution in double precision.

Propagation of a Solitary Wave

For a first test of the entire procedure, solitary waves were propagated across a level bottom. The waves used were actually pseudo-solitary, consisting of one wavelength of a regular wave with $L/d = 25$ superimposed upon a steady current which exactly opposed any return flow under the trough. Waves were propagated $25d$ using s time steps in an enclosed system of length $50d$. Figure 2 shows an example of water surface profiles as the wave propagated from left to right, and also serves as a definition sketch. Note the difference between d and d_s, the still water depths for the original periodic wave and the pseudo-solitary wave, respectively, and h_0 and h_s, the corresponding still water datums.

Since, in an enclosed box, the sum of kinetic energy, T, and potential energy, V, should remain constant over time, a single indicator of global accuracy was given by the Relative total Energy Fluctuations (REF). This was defined as

$$REF = \left((T+V)_{\max} - (T+V)_{\min}\right) / (T+V)_{t=0} .$$

Table 2 gives results for n values of 3, 7, and 11.

Trends are generally as expected; accuracy increasing with increasing degree of polynomial n, number of subdomains m, number of time steps s, and with decreasing wave height H/d_s. An interesting observation is that increasing n will not lower REF values if the computational grid in either space or time is too coarse. Similarly, if the solution to Laplace's equation is relatively inaccurate, a decrease in time step size will not give the expected convergence. Overall accuracy varies widely. In general, using n=3 appears to be only suitable for relatively small waves, while n values of 7 and 11 are suitable for the entire range tested. However, although highly accurate, the full potential of using n=11 does not appear to have been realised for this simple test, and it provides no clear advantage over a n value of 7.

To some degree, all computations showed growing fluctuations in total energy, although, as is readily obvious from REF values, these were generally quite small. The sawtooth instability of Longuet-Higgins and Cokelet (1976) was not observed in any of the cases in Table 2, although it could be reproduced if a coarser time step were used.

			REF			
H/d_s	n	m	s=75	s=150	s=300	s=600
	3	30	7.0×10^{-4}	2.0×10^{-4}		
0.1029	7	30	6.5×10^{-4}	9.1×10^{-5}		
	11	60		2.3×10^{-5}	1.0×10^{-6}	
	3	30	4.5×10^{-3}	2.2×10^{-3}		
0.2086	7	30	7.1×10^{-3}	7.6×10^{-3}		
	11	60		2.1×10^{-4}	7.1×10^{-6}	
	3	30	1.4×10^{-2}	1.1×10^{-2}		
0.3161	7	60		8.6×10^{-4}	7.7×10^{-5}	
	11	60		8.7×10^{-4}	8.8×10^{-5}	
	3	60		5.4×10^{-3}	4.7×10^{-3}	
0.4249	7	60		2.7×10^{-3}	1.1×10^{-3}	
	11	120			1.0×10^{-4}	3.2×10^{-6}
	3	60		1.2×10^{-2}	1.1×10^{-2}	
0.5346	7	120			3.3×10^{-4}	2.0×10^{-5}
	11	120			3.4×10^{-4}	1.1×10^{-5}

Table 2. Energy conservation during solitary wave propagation

Run times for 100 time steps with m=60 on a 80486 DX2-66 based PC were 16s, 87s, and 251s for n values of 3, 7, and 11, respectively.

Reflection of a Solitary Wave by a Vertical Wall

For a more demanding test, the interaction of two identical, oppositely directed solitary waves or, equivalently, the reflection of a solitary wave by a vertical wall was next modelled. The computational domain consisted of an enclosed system of length $50d$, with initial conditions of two inwardly directed solitary waves. For a given number of time steps, s, used in a computational run, the step size, Δt, was chosen such that the undisturbed solitary wave would propagate $25d$ in this time. Figure 3 shows a sequence of water surface profiles, ending near the centre of the interaction.

Several results of engineering interest may be obtained from these calculations: namely the maximum water surface elevation at the wall, the maximum force on the wall, and the maximum moment about the base of the wall. These are nondimensionalised as follows:

$$\eta^* = 1 + (\eta - h_s)/d_s .$$

$$F^* = \text{force per unit length} / \rho g d_s^2 ,$$

$$M^* = \text{moment about base per unit length} / \rho g d_s^3 ,$$

For all quantities, no attempt was made to interpolate between time steps to find the maximum value.

Results are summarised in Table 3. It is seen that, to keep errors small, discretisations in both space and time must be much finer than for the case of a propagating solitary wave. Computations could also become unstable using parameters which would successfully propagate a wave of the

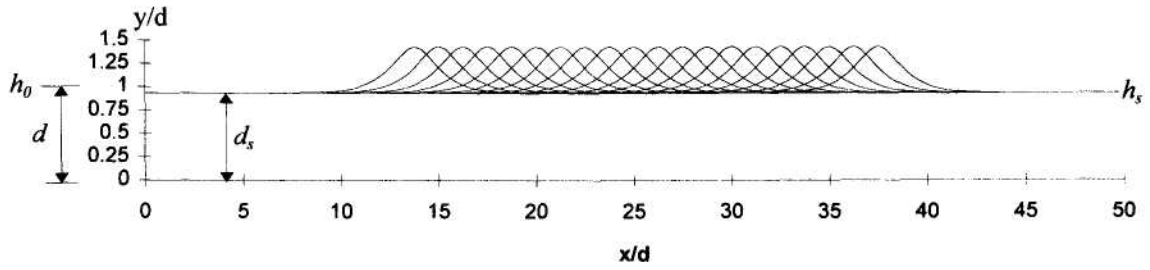

Figure 2. The propagation of a solitary wave of height 0.5346

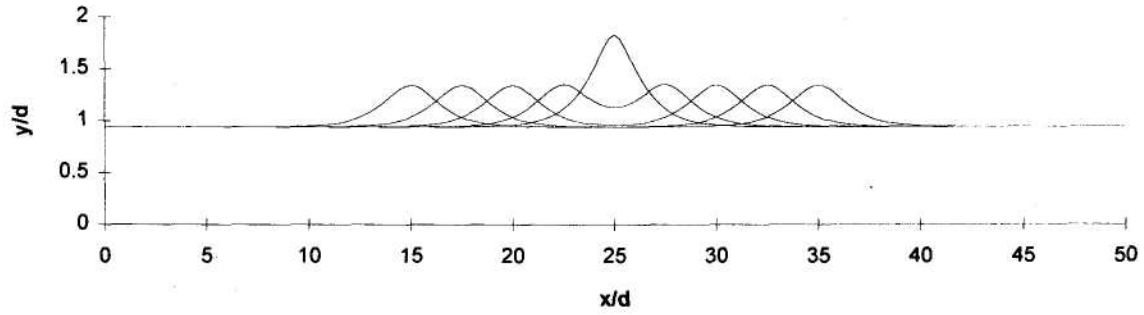

Figure 3. Surface profiles of colliding solitary waves of height 0.4249, ending near centre of interaction

H/d_s	n	m	s	F^*	M^*	η^*	REF
0.1029	7	120	600	0.7184	0.2893	1.2117	2.8×10^{-6}
0.2086	7	120	600	0.9553	0.4536	1.4436	6.1×10^{-5}
0.3161	7	120	600	1.1828	0.6467	1.7003	4.5×10^{-4}
0.4249	7	200	1000	1.3848	0.8435	1.9958	5.4×10^{-4}
0.5346	11	600	3500	1.6022	1.0598	2.3685	5.3×10^{-4}

Table 3. Maximum runup, force, and overturning moment arising from a solitary wave incident on a vertical wall

same height. In particular, obtaining an accurate solution for the highest wave tested required many attempts with increasingly fine discretisations. The growing periodic total energy fluctuations of the previous section were not as important here, since the largest energy variations invariably occurred near the centre of the interaction. It is possible that another time stepping procedure might improve things somewhat, as the AB4 scheme is relatively unstable. All of these findings were not entirely unexpected, as this is one of the most demanding problems involving nonbreaking waves.

One final aspect is worthy of mention. Forces and moments given here were nondimensionalised with respect to d_s, the solitary wave depth. However, the waves used, as stated in a previous section, were actually pseudo-solitary and formed from a regular wave with L/d=25. If the wave is regarded in this manner, and the equivalent regular wave depth, d ($>d_s$), is used to calculate dimensionless forces and moments, they can vary significantly from those in Table 3. For the highest wave tested, the maximum force drops by over twelve percent, while the maximum overturning moment is more than eighteen percent less than if the solitary wave depth d_s were used. For smaller waves, the difference is less. Since, in a real world situation, a wave impacting on a wall is likely to have more of a periodic than solitary nature, actual forces and moments for a nonbreaking design wave of height H/d are likely to be less than given here.

Shoaling of a Solitary Wave

As a final test of the LPA technique, the shoaling of a solitary wave of initial height 0.1029 was examined. The computational domain consisted of three sections: an initial level of depth d_s and length $25d$, a slope of the same length with depth decreasing cosinusoidally to a final shelf of depth d_f and length $50d$. As with the previous two test setups, the boundaries of the computational domain were taken to be vertical walls. The time step Δt was chosen so that the undisturbed wave would have travelled $90d$ in s time steps. Figure 4 gives some examples of propagation.

General features were common to both runs. On the first flat, the wave propagated without change of form. While passing over the slope, wave height increased slightly, the front of the wave steepened, and there were small reflections. Once on the final shelf, the wave continued to grow as the advancing mass split into what appeared to be several solitary waves of progression, with the highest at the front.

Results are qualitatively similar to solutions to the variable depth KdV equation by Johnson (1973), which show the wave mass on the final shelf fissioning into solitary waves followed by an oscillatory tail. However, due to assumptions inherent in the KdV equation, these solutions show no reflections, as were found here.

This test setup showed most clearly the limitations of the AB4 scheme. The growing fluctuations in energy observed while propagating solitary waves on a level bottom were a concern, and required fine discretisations to keep them

under control. Accuracy was further decreased by the continually increasing height to depth ratio as the wave progressed. Interestingly, fluctuations were in the kinetic energy, while the water surface profile seemed reasonable. The reason for this is unclear. Wave propagation into a depth of $03d_s$ could not be computed accurately with any discretisation tried, likely due to incipient breaking, which is beyond the capabilities of this scheme.

Conclusions

A method has been developed using local polynomial approximation to provide a highly accurate and efficient solution to Laplace's equation for potential flow in finite depths, and thus to simulate nonbreaking wave motion over varying topography for one dimension in plan. The use of a series of arbitrary order permits the choice of optimum parameters for a particular problem.

References

Dold, J.W., and Peregrine, D.H. (1984). Steep unsteady water waves: An efficient computational scheme. *Proc. 19th Conf. on Coastal Engineering,* Houston. ASCE., pp. 955-967.

Dommermuth, D.G., and Yue, D.K. (1987). A high-order spectral method for the study of nonlinear gravity waves. *J. Fluid Meek,* 184: 267-288.

Fenton, J.D. (1986). Polynomial approximation and water waves. *Proc. 20th Coastal Engineering Conf.,* Taipei, ASCE, pp. 633-646.

Fenton, J.D. (1988). The numerical solution of steady water wave problems. *Computers and Geosciences,* 14: 357-368.

Fenton, J.D., and Rienecker, M.M. (1982). A Fourier method for solving nonlinear water-wave problems: application to solitary wave interactions. *J. Fluid Mech.* 118:411-443.

Grilli, S.T., Subramanya, R., Svendsen, I.A., and Veeramony, J. (1994). Shoaling of solitary waves on plane beaches. *J. Waterway, Port, Coastal, and Ocean Engineering,* 120(6): 609-628.

Johnson, R.S. (1973). On the development of a solitary wave over an uneven bottom. *Proc. Cambridge Phil. Soc.* 73: 183-203.

Korteweg, D.J., and De Vries, G. (1895). On the change of form of long waves advancing in a rectangular canal and on a new type of long stationary waves. *Philos. Mag.* 39: 422-443.

Longuet-Higgins, M.S., and Cokelet, E.D. (1976). The deformation of steep surface waves on water 1. A numerical method of computation. *Proc. Roy. Soc. London A* 350: 1-26.

Multer, R.H. (1973). Exact nonlinear model of wave generator. *Journal Hydraulics Division ASCE,* 99: 31-42.

Nwogu, O., (1993). Alternative form of Boussinesq equations for nearshore wave propagation. *J. Waterway, Port, Coastal, and Ocean Engineering,* 119(6): 618-638.

Peregrine, D.H. (1967). Long waves on a beach. *J. Fluid Mech.,* 27(4): 815-827.

Rienecker, M.M., and Fenton, J.D. (1981). A Fourier approximation method for steady water waves. *J. Fluid Mech.,* 104: 119-137.

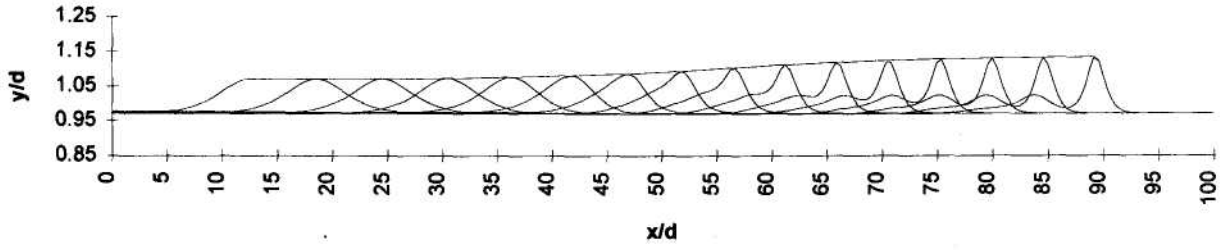

(a) d_f/d_s=0.5, n=7, m=240, s=1080, REF=7.2×10^{-4}

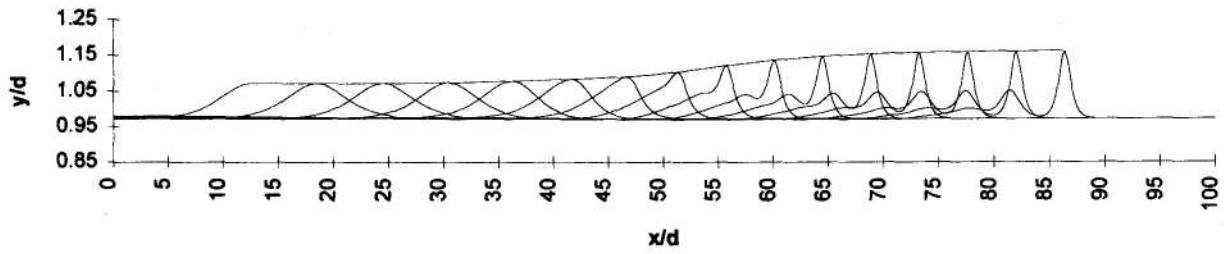

(b) d_f/d_s=0.4, n=7, m=480, s=2160, REF=3.3×10^{-4}

Figure 4. The propagation of a solitary wave onto a shelf